

# Protein folding classes — High-dimensional geometry of amino acid composition space revisited

"Too Many Molecules, Too Little Time"

— Ivan Amato, *Chemical and Engineering News*, March 9, 2006

Boryeu Mao

11328 179th Court NE  
Redmond, WA 98052  
USA

boryeu.mao@gmail.com

Running Title: Geometry of protein folding classes in amino acid composition space

Pages: 45 (including figures and tables)

Figures: 5

Tables: 4

Supplementary material: datasets for protein classes derived from SCOPe database

## Abstract

In this study, the distributions of protein folding classes of experimentally determined structures from a legacy dataset and a comprehensive database SCOPe are modeled with precise geometric objects as convex polytopes in the high-dimensional amino acid composition space. This is a follow-up of a previous non-statistical, geometry-motivated modeling of protein classes with ellipsoidal models, which are superseded presently in three important respects: (1) as a paradigm shift descriptive 'distribution models' of experimental data are de-coupled from, and serves as the basis for, future potential predictive 'domain models' generalizable to proteins in the same structure class for which the 3-dimensional structures have yet to be determined experimentally, (2) the geometric and analytic characteristics of class distributions are obtained via exact computational geometry calculations, and (3) the full data from a comprehensive database are included in such calculations, eschewing training set selection and biases. In contrast to statistical inference and machine-learning approaches, the analytical, non-statistical geometry models of protein class distributions demonstrated in this study, complete with precise information on the size of class distributions and their relative disposition in the high-dimensional space, and intended not principally for prediction but as accurate description of the complex relationships between amino acid composition and protein classes, suggest that they may ultimately be useful adjuncts for validating sequence-based methods for predicting protein structures and contribute to the mechanistic understanding of secondary structure formation and the folding of polypeptide chains into 3-dimensional conformation of functional protein molecules.

## Keywords

amino acid composition of proteins; secondary structure of protein conformation; protein classes and folding types; geometry in high dimensions; computational geometry; database of experimentally determined protein structures.

## Introduction

The sequence of 20 naturally occurring amino acids of the polypeptide chain constitutes the primary structure of a protein molecule. Short-range interactions among sidechains of neighboring amino acid residues along the polypeptide backbone lead to the local formation of secondary structure elements such as  $\alpha$ -helices and  $\beta$ -strands that further organize into tertiary motifs through long-range interactions among residues far apart along the polypeptide chain but brought to spatial proximity in the overall folded three-dimensional conformation. These tertiary motifs, also called protein structure domains, usually consists of a hydrophobic core with abundant contacts among elements within but weak or little interactions without. Three-dimensional protein structures at atomic resolution solved by x-ray crystallography or NMR spectroscopy show clearly recognized patterns in which  $\alpha$ -helices and/or  $\beta$ -strands are well packed into structural domains that have been categorized into different folding types, or classes, according to the content of predominant secondary structures: the class of  $\alpha$  or  $\beta$  if there are significant numbers of amino acid residues in either secondary conformation, or mixed classes of  $\alpha/\beta$  and  $\alpha+\beta$  if both are present [1,2]. These protein classes play a central role in understanding protein structure and function and evolutionary biology in general on the one hand, and physico-chemical forces driving the formation of secondary structures on the other. While the amino acid sequence (i.e. the order of different amino acid along the polypeptide backbone) is the primary determining factor in the formation of any local secondary structure element, the composition of amino acid residues without the order information is correlated with secondary structure content in protein structure [3,4], and the 20-component composition vectors span a quasi-continuum space ideal for geometric investigation of the relationship between protein classes and amino acid composition [5,6].

From distribution patterns of amino acid compositions of a curated basis set of protein structures then available, and a set of threshold criteria (of more than 15% of the amino acid residues in  $\alpha$  helix and less than 10%  $\beta$  strand for type  $\alpha$ , less than 15% in  $\alpha$  helix and more than 10%  $\beta$  strand for type  $\beta$ , and above both thresholds without dominance of either for mixed types), Nakashima et al. [5] showed that (1) the average of amino acid compositions of the  $\alpha$  class is distinctively different from that of  $\beta$ , and (2) protein structures of the different folding types are located in distinctive regions in the amino acid composition space each centered on the average of a given class with a root-mean-square (rms) radius. With the premise that the distribution of composition vectors of a given class is grouped together in the amino acid composition space, it was hypothesized that proteins meeting the threshold criteria for the type but outside the representative set, regardless of the specific content levels of the secondary structure [3,4], can be found in the corresponding region of the amino acid composition space, the region constituting the domain of influence for the forces underlying the formation of the secondary structures found in the folding type. Rules for determining the overall folding type of a protein molecule were then established based on the distance relationships of its amino acid composition vector relative to the class domains in the composition space.

In a subsequent study with similar geometric and non-statistical motivations [6], the product moment matrix of the amino acid compositions of the legacy basis set proteins of Nakashima, Nishikawa and Ooi ('NNO basis set') in a given class is diagonalized for deducing parameters of an ellipsoid in the composition space as a model of the class, and a modified, 'elliptically-scaled', distance measure was derived for classification criterion. In essence the two studies share the common idea of deriving a generally applicable distance measure for classification from the distribution of representative proteins of protein classes in the amino acid composition space, but arrive at different distance measures due to different protocols in constructing the amino acid composition space itself. In Nakashima et al. [5], the

components of the amino acid composition vector of a protein are calculated for the 20 naturally occurring amino acids relative to the overall averages and then normalized by their respective standard deviations, a procedure in which the relative scale of the 20 coordinate axes of the vector space, and consequently its metric, are effectively changed by the dataset-dependent normalization. In contrast, in Mao et al. [6] the plain amino acid compositions are used directly without normalization, for which the composition space is therefore only 19-dimensional, one degree of freedom fewer due to the single constraint that the 20 components sum to 1. Concomitantly, instead of effectively re-scaling coordinate axes of the vector space, an ellipsoid, a high-dimensional equivalent of an ellipse or hyper-ellipse, is derived from the *product moment matrix* of a distribution and its *diagonalization* (*pmmd* ellipsoid), which supplies geometric parameters for the 'elliptically-scaled' distance measure to programmatically account for the shape, size and the orientation of the distribution. The overall objective is to derive class models in the amino acid composition space from the basis set of protein structures, models that would include other proteins that the basis set may ostensibly be representing. Overlaps among the distribution models of folding types were recognized in both studies, and the intention of either an implicit spherical model [5] or more explicitly the 19-dimensional pmmd ellipsoid [6] was that relevant properties beyond size and shape, such as the overlap between distributions, may also be quantified analytically or computationally.

Although the overall objective of deriving class models is largely met with pmmd ellipsoidal geometry and the associated distance measure, two dissatisfying implications were clear and recognized at the outset: (a) given the conclusion that the high dimensional amino acid composition space will be inherently a sparsely inhabited space [6], a necessary requirement for improving folding type classification is a substantial increase in protein structural data of the basis set, and (b) the pmmd ellipsoid is a compound model with parameters that are part geometric information of the distribution

of basis set proteins and part projection for proteins that basis set proteins ostensibly represent, parts that might be unbundled for more robust and effective modeling of the protein folding classes. Advancing in these directions would await the emergence and progress of protein structure databases [7-9], as well as developments in computational geometry algorithms and methods [10-15]. In revisiting the high dimensional geometry of amino acid composition and protein folding types, in Section 1 of Results we argue for deferring the pmmd approach, and uncoupling modeling *data distributions of specific proteins* in the basis set from the conceptually and procedurally separable modeling of *class domains*, for *all proteins* which proteins in the basis set are intended to be representatives of. In this 'divide and conquer' approach, the distribution modeling would precede, and serve as the basis for, the more general and arguably more complex domain modeling. Continuing with plain amino acid compositions (i.e. without normalization), data distributions of protein folding classes in NNO basis set are then modeled with alternative and more suitable geometric models of minimum-volume enclosing ellipsoid [10] and convex polytope [12,14]. In Section 2, for improving the representation of protein classes in a basis set, protein data from SCOPe structural database [8,9] are parsed for data distributions of a comprehensive basis set. Models of the folding types are compared with those from NNO basis set in their geometry. Relevant questions to ask of the data distribution models are: location in the composition space, size and shape of the occupied space, and relative geometric disposition among classes, which may be: overlapping (inherently ambiguous and unresolvable folding types for certain amino acid compositions, the extent of which may suggest the need for alternative distribution models), or complete separation (unambiguous folding type designations according to amino acid composition).

Beyond protein classes, amino acid composition and related attributes has been found to be relevant to interesting aspects of protein structure, function and evolution [16-19]. A fundamental understanding

of the relationship between protein folding types and amino acid composition exemplified in the geometry of the high-dimensional space nevertheless would help in ultimately delineating the physico-chemical forces underlying and influencing secondary structure formation [4] and overall folding into the three-dimensional protein conformation [20].

For facilitating the presentation of materials, set notations are used throughout the text, and relevant routines and procedures are documented in pseudo code and collected in the Methods section. Actual codes, as well as datasets for the study, are available upon request. Data processing and computations were carried out on a Linux virtual machine (Debian 12 operating system) hosted in Qubes OS hypervisor (4.2.3) running on a Dell 3505 computer, with dual-core Ryzen 5 processor and 16 megabytes of memory.



# Results

## 1. Geometric Representation

In the pmmd approach for modeling the relationship between protein folding class and amino acid composition [6], it was hypothesized that the envelope of pmmd ellipsoid prescribes the domain boundary of the class in the amino acid composition space<sup>1</sup> within which the elliptically-scaled distance is a useful measure for classifying proteins to that class, a boundary where physico-chemical forces influencing the secondary structure formation in the folding type would be diminished and the amino acid composition no longer relevant for the folding type. In order for covering proteins outside of the basis set of the class, the hypothesized domain boundary might be expected to expand from the immediate neighborhood of data distribution (as shown for the pmmd ellipsoid for the 2D illustration in Figure 1). Hypothesis testing and refinement of the pmmd ellipsoid or similar models for class domains would be complex due to the lack of a full mechanistic understanding of the physical and chemical forces underlying the formation of secondary structures. A more effective alternative would be to re-cast the folding type classification problem, and uncouple modeling the data distribution of specific proteins of a class in the basis set from domain modeling appropriate for all proteins of that class, with separate hypothesis testing and validation as necessary; that is, deferring compound model such as pmmd ellipsoid in favor of a descriptive model of data distribution of basis set proteins and a conceptually and procedurally separate domain model.

<sup>1</sup> Amino acid compositions are fractions calculated from integer counts of individual amino acids and their sum. Accordingly, the amino acid composition space is the space of rational numbers, denoted as  $\mathbb{Q}^n$ , spanned by 20 axes, each consisting of discrete rational numbers in the interval  $[0,1]$  and representing a naturally occurring amino acid, subject to the constraint that the 20 components sum to 1. Protein classes occupy parts of the amino acid composition space that are compositions realizable by proteins of finite lengths with length distributions genomically specified in proteomes.

Following the class designation of 1 to 5 [6], data distributions of classes for NNO basis set are denoted as follows:

$$\text{class}(i) := \{ \text{amino acid composition vector } \bar{v} \text{ of protein} \mid \text{protein} \in \text{FT}(i) \}, \text{ where}$$

$$i \in \{1,2,3,4,5\}, \text{FT}(i) \in \{\alpha, \beta, \alpha/\beta, \alpha+\beta, \text{irregular}\},$$

with the cardinality of the classes, denoted with collective term  $\mathbf{I} := \{1,2,3,4,5\}$ :

$$N(\text{class}(\mathbf{I})) := \{29,34,39,26,4\}.$$

Formal definitions of sets and functions and procedures for geometric calculations, as well as symbols, notations are found in Methods section.

For the purpose of a suitable and more precise descriptive model of class distribution, the 'loosely fitting' pmmd ellipsoid conceivably could be scaled inward radially such that its envelope comes in contact with the outer-most data points in the distribution (i.e. vertices in Figure 1). This however will not be the smallest such ellipsoid except in special cases (when the distribution is symmetrical, for example). Instead, for a strictly smallest and hence more precise descriptive model covering a distribution, a well-known algorithm is the **minimum volume enclosing ellipsoid (mve ellipsoid)** [10], and the python code for arbitrary dimensions is available and published in github.com [11]. Results of pmmd ellipsoid  $P(\mathbf{J})$ , reproduced for backward reference and for comparison, and mve ellipsoid  $M(\mathbf{J})$  for  $\mathbf{J} := \{1,2,3,4\}$  are shown in Table I. Rather than floating point numbers in percentage unit before [6], components of the amino acid composition vector are now fractions in the rational number form, and thus the volume in 19D [6,21 and Methods] smaller by a factor of  $10^{-38}$ , in slightly higher numerical precision due to computing in rational number arithmetic.

Table I

As illustrated in Figure 1, an mve ellipsoid is a more precise representation of a point distribution than pmmd ellipsoid due to its reduced envelope, but an even more and ultimately the most concise geometric form is that of convex polytope, essentially a shrink-wrap around the point set, and an extensively researched and active field of study [12,14]. Unlike pmmd ellipsoid, both mve ellipsoid and polytope are essentially defined by the boundary of the distribution; any internal structure (i.e. the 7 interior points in Figure 1) or any duplicate data points are 'redundant' in that they do not change the geometric object. A convex polytope, as exemplified by the polygon, a 2D polytope, shown in Figure 1, is the region in real space  $\mathbb{R}^n$  defined by its set of vertices, or equivalently bounded by a set of facets (i.e. line segments in 2D between neighboring pairs of vertices) that collectively form the envelope covering the point set. Lines extending from the facets (in long dashes) are half planes which are duals of vertices defining the polytope [12,14]. For the purpose of this study, three groups of computational geometry calculations are defined for a polytope model  $T$  of a distribution  $\underline{D}$  [Methods II(a)]: (1) a redundancy test,  $\text{redund}(\underline{D})$ , to identify points that are 'redundant' in its definition, and  $\text{vertex}(\underline{D})$ , for the remainder in  $\underline{D}$  that are non-redundant and essential; (2) inter-conversions between dual representations  $T_v$  and  $T_h$  of polytope in vertices and in half-planes respectively; and (3) from  $T_v$ , a computation of the content of a polytope ('area' for 2D polygons, 'volume' for 3D polyhedra, and generalized to 'hyper-volume' for higher dimensional polytopes). As the computing resources required for polytope calculations scale combinatorically with the number of points in the distribution, mve ellipsoid is an useful surrogate where polytope calculations become prohibitively expensive. The basic concepts of computational geometry calculations relevant to this work are outlined and illustrated

---

<sup>2</sup> It is worth noting that the geometry of rational coordinate space  $\mathbb{Q}^n$  is limited (for example, the distance is in general real and not rational). Thus by necessity the amino acid composition space is embedded in the real coordinate space for modeling the protein classes as geometric object in  $\mathbb{R}^n$ .

schematically in Figure 1 and Figure 2. Readers are referred to computational geometry texts and resources for further details.

Geometric parameters computed for the four main folding types  $\text{class}\langle\mathbf{J}\rangle$  are shown in Table I.

Compared to the 2D example in Figure 1, the volume reduction from pmmd ellipsoid to mve ellipsoid and to polytope is more pronounced in 19D. For NNO basis set, all  $\text{redund}(\text{class}\langle\mathbf{J}\rangle)$  is null, or equivalently,  $\text{vertex}(\text{class}\langle\mathbf{J}\rangle)$  and  $\text{class}\langle\mathbf{J}\rangle$  are identical; that is, all representative proteins are vertices of their respective polytopes, without any redundancy or interior points.

Figure 2

For two distributions  $\underline{D}_1$  and  $\underline{D}_2$ , any intersection of their polytope representations<sup>3</sup> that might exist can be readily evaluated in a relatively straightforward vertex enumeration  $\underline{Q}_p(\underline{D}_1, \underline{D}_2)$  [Methods II-4], since the region of intersection is itself a polytope, as shown schematically in orange in Figure 2. For polytope in high dimensional space of even only a few vertices, the combinatorial increase in the number of half-planes (Table I) would require significant dedicated computer resources (processor speed, core size and disk storage) for direct computation of  $\underline{Q}_p$ . As an economizing and practical alternative, provisional overlap information can be deduced from examining the following types of discrete overlap [Methods II(b)], in the order of decreasing proximity: full and partial centroid overlap  $\underline{Q}_c(\underline{D}_1|\underline{D}_2)$ , distribution overlap  $\underline{Q}_d(\underline{D}_1|\underline{D}_2)$ , as illustrated in Figure 2.

Among  $\text{class}\langle\mathbf{J}\rangle$ , all  $\underline{Q}_c$  and  $\underline{Q}_d$  are null. However the distributions may not be completely separated from one another since there may still be facet overlaps (e.g. two prisms in contact at edges and faces)

---

<sup>3</sup> The polytope intersection, as defined in Methods II-4, is distinct from the intersection of the distributions themselves, which is defined as the set of any common members, that is, amino acid compositions that appear in both distributions. This common set can be identified without polytope computations, and may be considered as a more fundamental overlap than polytope overlaps. No intersections exist among classes in NNO dataset.

that must be ultimately evaluated with polytope  $\mathcal{Q}_p$ . For classes 1 and 4 for example, with the smallest combined set of half-planes (Table I, row 7), the preliminary result of  $\mathcal{Q}_p(\text{class}\langle 1 \rangle, \text{class}\langle 4 \rangle)$ , a month-long vertex enumeration calculation on dedicated hardware courtesy of David Avis, shows that the two distributions do indeed overlap ( $\mathcal{Q}_p(\text{class}\langle 1 \rangle, \text{class}\langle 4 \rangle)$  is not null). To summarize, class distributions of NNO basis set proteins are intersecting only on the periphery, implying that overlaps of pmmd ellipsoids observed previously [6] are overlaps of hypothesized class domains.

Given that  $\text{redund}(\text{class}\langle \mathbf{J} \rangle)$  is null for all  $\mathbf{J}$ , proteins in NNO basis set define only the polytope boundary for the classes but are too few for any internal occupancy, arguably an indication that they are poor overall representations of the folding classes: the distributions are either 'small' and 'thin', or otherwise 'superficial' without internal quasi-continuum, to adequately support claiming and hypothesizing class domains for representing the folding types more widely. These considerations point to expanding the protein basis set for remedying the poor data representation, perhaps by way of a database approach, instead of revising or augmenting NNO basis set with risks of implicit or hidden biases that are often associated with training set selections.

## 2. Protein Database

CATH [7] and SCOPe [8,9], two major comprehensive, hierarchical protein structure databases were initially developed and available in mid- to late-1990's and continuously evolving since. Both databases collect 3D protein structures from Protein Data Bank (PDB), <https://www.rcsb.org>, a repository of experimental structure data from x-ray crystallography or NMR spectroscopy, and in conjunction with genetic and sequence information derive a classification hierarchy of evolutionary and functional relationships among proteins. In both databases, the classification at the top level identifies

the folding types according to the predominant secondary structure content of  $\alpha$  helices and/or  $\beta$  strands. Structures with mixed  $\alpha$  and  $\beta$  are grouped into a single class in CATH [22], but separately into two classes  $\alpha/\beta$  and  $\alpha+\beta$  in SCOPe [23] similar to classification studies before [5,6] and thus more suited as an expanded basis set for the folding types<sup>4</sup>. In the 7-level hierarchy of SCOPe (Figure 3), the major classification is encoded in an alpha-numeric SCOPe concise classification string (**sccs**), in the form of **cl.cf.sf.fa** for the top four levels of **Class**, **Fold**, **Superfamily**, and **Family** respectively. At the 7th and the lowest level of SCOPe hierarchy are protein structure domains **px**, regions in the 3D protein conformation within which amino acid residues are well-packed into a structural core via optimal and stabilizing residue-residue interactions. The **px** entries, being the unit of classification in SCOPe [23] and identified by a 7-character **sid** string containing the associated PDB ID, correspond to members of NNO basis set. Evolutionarily related proteins and their structure domains are grouped into families at level **fa** [24], which then are organized into higher levels up to **Class** (level **cl**). Many structure domains are single-domain proteins of single polypeptide chains, while others are multiple domains within certain long polypeptide chains, or yet ones consisting of more than one polypeptide chain.

SCOPe parseable files [dir.cla.scope.txt](#) and [dir.com.scope.txt](#) [25], and its ASTRAL sequence resource file [astral-scopedom-seqres-gd-all-2.08-stable.fa](#) [26] are downloaded for version 2.08 of the database with 2023-01-06 updates. A small number of amino acid sequences not in the ASTRAL file are fetched from SCOPe individually [27]. In addition to the four major SCOPe classes, a, b, c, and d, corresponding to  $\alpha$ ,  $\beta$ ,  $\alpha/\beta$  and  $\alpha+\beta$  respectively, also included in this study is class g, a group of small proteins without significant secondary structures but stabilized by disulfide bonds or metal ion

<sup>4</sup> For the purpose of expanding the basis set for protein classes, experimental databases remain the 'gold standard', and prediction databases such as AlphaFold (of millions of structures) [20] may be useful complement when fully automated class assignment protocols become available (see Discussion).

chelation. Pre-processing of SCOPe data and statistics are detailed in Table II-a and II-b respectively.

Data distributions for the folding classes (Table II-b, row 4) are denoted as follows:

Figure 3

$$\begin{aligned} \underline{\text{class}}\langle k_0 \rangle &:= \{ \text{amino acid composition vector of } \mathbf{px} \mid \text{sid of } \mathbf{px} \in \text{SCOPe class } k \}, \text{ where} \\ k &\in \{a,b,c,d,g\}, \text{ SCOPe-folding-type}(k) \in \{\alpha, \beta, \alpha/\beta, \alpha+\beta, \text{small proteins}\} \\ N(\underline{\text{class}}\langle k_0 \rangle) &\in \{32957, 55705, 53404, 56681, 6007\} \end{aligned}$$

with collective terms  $\underline{\text{class}}\langle \mathbf{K}_0 \rangle$ ,  $\mathbf{K}_0$  and  $\mathbf{L}_0$  defined similarly to those for NNO basis set. With  $N(\underline{\text{class}}\langle \mathbf{K}_0 \rangle)$  being 3 orders of magnitude larger than NNO basis set, full computational geometry calculations would require significant hardware resources in processor speed, core memory, and disk storage<sup>5</sup>. For reducing resource needs, however, we make use of the hierarchical data structure and bootstrap<sup>6</sup> from a higher SCOPe level; for example, for distributions of folding classes  $k \in \{a,b,c,d,g\}$  at the **Protein** level (**dm**),

$$\underline{\text{protein}}\langle u \rangle := \{ \text{amino acid composition vector of } \mathbf{px} \mid \text{sid of } \mathbf{px} \in \text{SCOPe sunid-dm } u \},$$

where sid is the 7-character alphanumeric string that identifies a protein domain  $\mathbf{px}$ , and sunid-dm is the SCOPe internal unique numeric identifier **sunid** (<https://scop.berkeley.edu/help/ver=2.08>) for members of the hierarchy at the sixth level **dm** (Figure 3). With  $N(\{\underline{\text{protein}}\langle u \rangle \mid u \in \text{class } k\})$  of 2285,2333,2773,2966,743 respectively (Table II-b, row 5), which are lower than  $\underline{\text{class}}\langle \mathbf{K}_0 \rangle$  (Table II-b, row 4), though still 2 orders of magnitude larger than  $\underline{\text{class}}\langle \mathbf{I} \rangle$  (Table-I, row 6), not to mention combinatorically higher counts expected for half-planes. The situation becomes more manageable at the **Family** level (**fa**):

$$\underline{\text{family}}\langle s \rangle := \{ \text{amino acid composition vector of } \mathbf{px} \mid \text{sid of } \mathbf{px} \in \text{SCOPe sccs-fa } s \},$$

<sup>5</sup> To paraphrase Ivan Amato: "Too Many **Protein** Molecules, Too Little **Computer** Time."

<sup>6</sup> Bootstrapping, as in 'Leveraging a small, initial effort', here unrelated to bootstrapping operations of resampling in statistics.

with  $N(\{\text{family}\langle s \rangle \mid s \in k.*.*.*\}) \in \{893, 766, 807, 1093, 230\}$ , for  $k \in \mathbf{K}$  (Table II-b, row 6). Class distributions are derived from  $\text{family}\langle s \rangle$  as follows [Methods I, II]:

$$\text{Family}\langle s \rangle := \text{vertex}(\text{family}\langle s \rangle) \quad (\text{when } \text{vertex}(\text{family}\langle k \rangle) \neq \text{family}\langle k \rangle)$$

$$\text{class}\langle k \rangle := \{\overline{\text{centroid}(\text{Family}\langle s \rangle)} \mid \text{SCOPE sccs-fa } s \in k.*.*.*\}$$

$$\text{Class}\langle k \rangle := \text{vertex}(\text{class}\langle k \rangle) \quad (\text{when } \text{vertex}(\text{class}\langle k \rangle) \neq \text{class}\langle k \rangle)$$

$$\overline{\text{centroid}\langle k \rangle} := \text{mean}(\text{Class}\langle k \rangle).$$

For folding type  $\alpha$ , for example, distribution  $\text{class}\langle a_0 \rangle$ , of 32957  $\mathbf{px}$ 's, is refactored hierarchically into  $\text{class}\langle a \rangle$  of the centroids of 893  $\mathbf{fa}$ 's, with  $N(\text{family}\langle s \rangle)$  ranging from 1 to 2750 and  $N(\text{Family}\langle s \rangle)$  from 1 to 528 (Table II-b, rows 7 and 8 respectively). Figure 2 schematically shows the relationship between  $T_v(\text{Class}\langle k \rangle)$  (polytope in blue), two of its  $\text{Family}\langle s \rangle$  (marked by blue  $\mathbf{x}$ ), and partial  $T_v(\text{Class}\langle k_0 \rangle)$ . (short dashed lines in blue). The choice of **Family** level as an effective unit of classification for protein folding types is also justifiable by its unique position in the hierarchy of protein structure, function and evolution [2,23]. The wide range of values for  $N(\text{family}\langle s \rangle)$  (Table II-b) reflects the great diversity in protein families. For relatively small  $\text{Family}\langle s \rangle$  ( $N(\text{Family}\langle s \rangle) < 51$ ),  $V_T$  are readily calculated and shown to correlate with  $V_M$  over 30 orders of magnitude (Figure 4), in essence a demonstration that an ellipsoid can mve-cover many different polytopes. The empirical correlation relationships are useful for estimating  $V_T$  of polytopes with high vertex count, for which  $V_M$  is more readily calculated and the value falls within range of the observed correlation regime appropriate for extrapolation.

The dataset size of  $\text{class}\langle \mathbf{K} \rangle$  (Table III-a) is significantly larger than NNO basis set, with approximately 20- to 30-fold increase from  $N(\text{class}\langle \mathbf{I} \rangle)$ ; for folding type  $\alpha$  for example,  $N(\text{class}\langle a \rangle)$  is 893, with 824



vertices ( $N(\text{Class}\langle a \rangle)$ ). Also, significantly larger than  $\text{class}\langle 5 \rangle$ ,  $\text{class}\langle g \rangle$  is now full rank. The comparison of distinctively different amino acid compositions of folding types  $\alpha$  and  $\beta$  for NNO basis set (Figure 5, top panel for  $\text{class}\langle 1 \rangle$  and  $\text{class}\langle 2 \rangle$ , and comparable to Figure 1 in [5]), shows that, geometrically speaking,  $\overline{\text{centroid}}\langle 1 \rangle$  and  $\overline{\text{centroid}}\langle 2 \rangle$  are located respectively in quadrants II and IV of the coordinate plane the origin of which is located at the overall mean of  $\text{class}\langle \mathbf{I} \rangle$  and one of the two axes parallel to the collective axis from amino acids  $\{K,A,E,M,H,L,D\}$  and the other to that from  $\{N,Y,V,P,G,C,T,S\}$ , the two groups of amino acids favoring  $\alpha$  helices (amino acid letter codes in blue) and  $\beta$  strands (letter codes in orange) respectively.

Similar to  $\text{class}\langle 1 \rangle$  and  $\text{class}\langle 2 \rangle$ , the amino acid compositions of  $\text{Class}\langle a \rangle$  and  $\text{Class}\langle b \rangle$  are shown to be distinctively different (Figure 5, bottom panel). Changes in the order of amino acids within the left and the right halves (primarily L,E,A,K,M for  $\alpha$  and N,S,P,T,V,G for  $\beta$ ), however show that directional vectors of types  $\alpha$  and  $\beta$  are re-oriented from those for  $\text{class}\langle 1 \rangle$  and  $\text{class}\langle 2 \rangle$ , but remain essentially in the respective quadrants, suggesting that the expansion of the legacy basis set proteins to a whole database refines but does not substantively alter the geometric relationship between folding types  $\alpha$  and  $\beta$ . Similar collective amino acid compositions were previously noted to correlate with  $\alpha$  helix content estimated from optical rotary dispersion measurements predating modern day x-ray diffraction and NMR spectroscopy [3,4].

Compared to NNO basis set, data distributions of  $\text{class}\langle \mathbf{L} \rangle$  occupy wider regions in the amino acid composition space, i.e.  $V_M(\mathbf{L}) > V_M(\mathbf{J})$  (Table III-a, row 2 vs Table I, row 3), and  $V_{T\text{-est}}(\mathbf{L}) > V_T(\mathbf{J})$  (last rows, Table III-a vs Table I).  $M\langle \mathbf{L} \rangle$  are less eccentric than  $M\langle \mathbf{J} \rangle$ . In contrast to NNO dataset,  $\text{redund}(\mathbf{K})$  is not null (Table III-b, row 1), e.g. of the 893 families of  $\text{class}\langle a \rangle$ , 69 are located in the

interior of  $T\langle a \rangle$ . Except for  $\text{class}\langle g \rangle$ , the interior subsets themselves are single-layer polytopes, and nearly concentric with their respective  $T\langle K \rangle$ . These results show that, by virtue of both outward and inward expansion of the distributions, SCOPe database improves the overall representation of the protein folding classes. As illustrated in Figure 2, the envelopes of  $T_v(\text{Class}\langle K_0 \rangle)$  (short dashed lines in blue) are expanded from the penultimate  $T_v(\text{Class}\langle K \rangle)$  (solid lines in blue). The average size of **Family** distributions (marked by x in Figure 2),

$$\text{mean}(\{\dim_M(\text{Family}\langle s \rangle) \mid s \in \text{Class}\langle k \rangle\})$$

are {0.0183, 0.0183, 0.0135, 0.0173} respectively for  $\text{Class}\langle L \rangle$ , equivalent to increases of {12.6%, 13.2%, 14.1%, 12.8%} (relative to  $\dim_M(\text{Class}\langle L \rangle)$ , Table III-a, row 4) of  $V(\text{Class}\langle L \rangle)$  for the estimated  $V(\text{Class}\langle L_0 \rangle)$ .

Table IV

As a result of the larger volume of  $\text{class}\langle L \rangle$  compared to  $\text{class}\langle J \rangle$ , and perhaps secondarily re-orientation of the distributions (Figure 5), there are now distribution overlaps<sup>z</sup> among the classes (Table IV-a), and centroid overlaps with  $\text{Class}\langle c \rangle$  or  $\text{Class}\langle d \rangle$  but not between  $\text{Class}\langle a \rangle$  and  $\text{Class}\langle b \rangle$  (Table IV-b). Note however that there are no overlaps of either type between any of  $\text{class}\langle L \rangle$  with  $\text{class}\langle g \rangle$ . For each  $\text{class}\langle k \rangle$ , the distribution overlaps with all other classes (last row, Table IV-a) constitute a fraction of its total, namely,  $N(\{O_d(\text{class}\langle k \rangle \mid \text{Class}\langle k' \rangle) \mid k' \neq k\}) < N(\text{class}\langle k \rangle)$ , or, in other words, the remainder of  $\text{class}\langle k \rangle$  are located in non-overlapping part(s) of  $T\langle k \rangle$  unique to the class. In particular,  $T\langle c \rangle$  and  $T\langle d \rangle$  (and estimated  $T\langle c_0 \rangle$  and  $T\langle d_0 \rangle$ ), though clustered close together, do not completely overlap with each other, in support of two separate classes for  $\alpha/\beta$  and  $\alpha+\beta$  as in SCOPe

<sup>z</sup> As noted before, the distribution overlaps here refer to overlaps between polytope representations of the distributions. For the intersection between distributions of the SCOPe dataset, there are often replicate amino acid compositions within a family, due to proteins from different species for example, which are treated as 'redundant'. Only three amino acid compositions are common between different families: two for b.1.1.1 and b.1.1.2, and one for b.40.4.5 and b.40.4.11, and more importantly, no common amino acid compositions exist between classes.

[23,28], rather than a combined mixed  $\alpha$  and  $\beta$  class as in CATH [7,22]. The eventual complete calculation for full distributions  $\underline{O}_p(\underline{\text{class}}\langle c_0 \rangle, \underline{\text{class}}\langle d_0 \rangle)$  will determine if class  $\alpha/\beta$  falls completely within, and therefore a subset of  $\alpha+\beta$ .

Centroid-to-centroid distances among  $\underline{\text{class}}\langle \mathbf{L} \rangle$  are shown in Table IV-b (rows 1-5):  $T\langle a \rangle$  and  $T\langle b \rangle$  are farthest apart, at a distance of 0.0696,  $T\langle c \rangle$  and  $T\langle d \rangle$  closest together at a distance of 0.0171, while  $T\langle g \rangle$  is located far away, at distances greater than 0.1 from, and not overlapping with,  $T\langle \mathbf{L} \rangle$ . Of the four major folding types,  $T\langle d \rangle$  is located virtually at the center  $\overline{\text{centroid}}(\overline{\text{centroid}}\langle \mathbf{L} \rangle)$  (Table IV-b, row 6). At equal distances from  $T\langle d \rangle$  that sum up to approximately the  $T\langle a \rangle$ - $T\langle b \rangle$  distance,  $T\langle a \rangle$  and  $T\langle b \rangle$  are located diametrically from the group center, consistent with Figure 5. Given full bipartite centroid overlaps among  $T\langle b \rangle$ ,  $T\langle c \rangle$  and  $T\langle d \rangle$ , and nearly full bipartite centroid overlaps among  $T\langle a \rangle$ ,  $T\langle c \rangle$  and  $T\langle d \rangle$ , (the only exception being  $T\langle a \rangle$  and  $T\langle c \rangle$ ), classes b,c,d are clustered slightly more tightly than classes a,c,d, with a triangular area of the centroids of the b,c,d-cluster, or  $V_T(\{\overline{\text{centroid}}\langle k \rangle \mid k \in \{b,c,d\}\})$ , of 6.130e-6, compared to 7.316e-6 for  $V_T$  of the a,c,d-cluster. Together these geometric parameters are summarized in the following clustering relationship of  $T\langle \mathbf{K} \rangle$  in order of decreasing proximity:

$$T\langle c \rangle, T\langle d \rangle > T\langle b \rangle, T\langle c \rangle, T\langle d \rangle \gtrsim T\langle a \rangle, T\langle c \rangle, T\langle d \rangle > T\langle a \rangle, T\langle b \rangle > T\langle g \rangle, T\langle \mathbf{L} \rangle$$

For class g, a group of proteins with little or no  $\alpha$  or  $\beta$  secondary structures,  $T\langle g \rangle$  is located in the amino acid composition space far away from  $T\langle \mathbf{L} \rangle$  (Table IV-a) and also at a large distance to  $\overline{\text{centroid}}(\overline{\text{centroid}}\langle \mathbf{L} \rangle)$  (Table IV-b), that is, amino acid compositions of proteins in class g are significantly different from those with  $\alpha$  or  $\beta$  secondary structures and thus as a group is a proper

negative control for associating amino acid composition in the region around  $\text{class}\langle\mathbf{L}\rangle$  with  $\alpha$  helix or  $\beta$  strand secondary structure formation.

Relative to SCOPe release 2.07, database additions and updates in release 2.08 (Table II) did not substantively alter the geometric dispositions of the folding classes (Table IV-b, row 8).

Compared to distances among  $T\langle\mathbf{L}\rangle$  for SCOPe database (Table IV-b, rows 1-6), the corresponding values for  $T\langle\mathbf{J}\rangle$  in NNO basis set are larger, which is consistent with a slightly exaggerated difference between folding types  $\alpha$  and  $\beta$  (Figure 5), and quantified as:  $V_T(\overline{\text{centroid}\langle\mathbf{J}\rangle}) > V_T(\overline{\text{centroid}\langle\mathbf{L}\rangle})$ , at  $1.379\text{e-}7$  and  $2.783\text{e-}9$  respectively. In reference to class distributions in SCOPe individually on the other hand, NNO basis set proteins populate the domains only sparsely and non-uniformly (small  $N(\text{class}\langle\mathbf{J}\rangle)$ ), covering only small sub-regions (smaller  $V_T$  or  $V_M$  than  $\text{class}\langle\mathbf{L}\rangle$ ), and off-centered (Table IV-b, row 7).

## Discussion

For classification of protein folding types, the distributions of specific proteins in the legacy NNO basis set of Nakashima et al. [5] in the amino acid composition space are re-modeled with computational geometry models. Although there is little or no intersection among the distributions (i.e., distinctively different amino acid compositions for the four main folding types), the basis set distributions are too small, in both set cardinality and volume content, and inherently limited to be fully representative of the folding classes. Datasets from SCOPe database on the other hand not only substantively expand the coverage of the folding type domains for the four main folding types but also natively furnish a fifth group, of small proteins with little or no  $\alpha$  helix or  $\beta$  strand secondary structures, as a proper negative control. The results show that for data distributions of SCOPe basis set, folding type  $\alpha+\beta$  is located near the center of the four main folding types in the amino acid composition space, clustered closely with the most compact distribution of class  $\alpha/\beta$  and flanked by classes  $\alpha$  and  $\beta$ . Computational geometry modeling of data distributions from the SCOPe database overcomes limitations of the smaller NNO basis set, and also addresses long-standing open questions in the previous study [6].

The geometry of the distributions of protein classes in the high dimensional space accurately demonstrated the complex relationship between folding types and amino acid compositions, which is necessary for developing predictive models and could be an useful adjunct for validating sequence-based protein structure prediction (AlphaFold and others). The geometry-motivated whole-database approach may also contribute to the mechanistic understanding of the formation of secondary structures in protein conformation (the four main classes vs. the class of 'small proteins'), and possibly even more broadly to proteomics (folded vs. disordered protein molecules [29], for example).

SCOPe undergoes periodic updates, as newly released protein structures in PDB databank are incorporated into the database. Although there are only small increments in the dataset from SCOPe release 2.07 to 2.08 (Table II), with minimum effects on the overall geometry of the folding classes (Table IV-b, row 8), a trend to be expected for a maturing database, any addition of unusual structures in a particular release may be detected by continually monitoring the geometry of class distributions.

In addition to periodic updating, further work of interest on data distributions of protein classes include:

(1) with sufficient computing resources, full computations for  $\text{class}\langle\mathbf{K}\rangle$  and  $\text{class}\langle\mathbf{K}_0\rangle$ , which would allow further testing of the distribution model hypothesis for the classes; (2) re-constructing quasi-amino acid composition space in collective amino acid compositions, such as {L,E,A,K,R} and {P,T,V,G} (Figure 5), that would lower the effective dimension of the geometric space,  $r$ , and consequently (a) decrease  $N(T_v)$  and  $N(T_h)$ , and the resource requirements for full computational geometry calculations, and (b) increase  $\sqrt[r]{N}$ , the mean 'linear density' of  $N$  points along coordinate axes of an  $r$ -dimensional space, and the population density of data distribution in the geometric space; (3) surveying Protein Data Bank for an optimal set of criteria of secondary structure content, such as 15% of the amino acid residues for  $\alpha$  helix and 10% for  $\beta$  strand [5], for robust and automatic classification of the folding type of protein structures that are either experimentally determined [7-9] or computationally predicted [20]; (4) cross-referencing protein folding classes in SCOPe and CATH databases.

## Methods

### I. General

A distribution  $\underline{D}$  (with underline) is a set of 20-component vectors  $\bar{v}$  (with overline) belonging in a defined group  $G$

$$\underline{D} := \{ \bar{v} \mid \bar{v} \in G \}$$

where  $\bar{v}$  is located in the 19D hyper-plane that intersects the 20 coordinate axes at unit distances from origin, either a proper amino acid composition vector of fractions of the counts of 20 naturally occurring amino acids to the total residue count of a protein, or one derived from such amino acid composition vectors. A list of properties and geometric quantities of  $\underline{D}$  includes

$N(\underline{D})$	cardinality of distribution $\underline{D}$ , a set of vectors
$P(\underline{D}) := pmmd(\underline{D})$	ellipsoid derived from product moment matrix diagonalization procedure <i>pmmd</i> [6]
$M(\underline{D}) := mvee(\underline{D})$	minimum volume enclosing ellipsoid from procedure <i>mvee</i> , python code for arbitrary dimension published in <a href="https://github.com">github.com</a> [11]

$$V_X(\underline{D}) := (\pi^{1/2} / \Gamma(1+r/2)) \cdot \prod r_m(X(\underline{D})), \quad X \in \{P, M\}$$

volume of ellipsoid  $X$ , of rank  $r$  and  
radii  $r_m(X(\underline{D}))$  for distribution  $\underline{D}$ ,

$\Gamma$  is the gamma function and  $\prod r_m$  is the product of  
all radii,  $r_m$  [6,21]

$$\dim_M(\underline{D}) := \sqrt[r]{(V_M(\underline{D}) / (\pi^{1/2} / \Gamma(1+r/2)))}$$

geometric mean of the radii of mve ellipsoid

of rank  $r$ , as an estimated size per dimension  
of  $\underline{D}$  suitable for comparison of distributions  
of different rank

and collective terms,

$\mathbf{I} := \{1,2,3,4,5\}$  and  $\mathbf{J} := \{1,2,3,4\}$  for all classes and four main folding types,

respectively, in NNO basis set

$\mathbf{K} := \{a,b,c,d,g\}$  and  $\mathbf{L} := \{a,b,c,d\}$  for classes in SCOPe database

$\text{class}(\mathbf{X}) := \{ \text{class}(i) \mid i \in \mathbf{X} \}, \mathbf{X} \in \{ \mathbf{I}, \mathbf{J}, \mathbf{K}, \mathbf{L} \}$  distributions for classes in  $\mathbf{X}$

$M(\mathbf{X}) := M(\text{class}(\mathbf{X})), \mathbf{X} \in \{ \mathbf{I}, \mathbf{J}, \mathbf{K}, \mathbf{L} \}$  mve ellipsoid  $M$ , and similarly for other  
properties or quantities

## II. Polytope

(a) Three groups of calculations for a polytope model  $T$  of distribution  $\underline{D}$  :

1. Redundancy test to identify points that are duplicates, located within the interior of  $T$ , or otherwise  
'redundant' in its definition,

$\text{redund}(\underline{D}) := \{ \bar{v} \mid \bar{v} \in \underline{D} \ \& \ \bar{v} \in \text{redundancy}(\underline{D}) \}$  set of redundant vectors, itself a distribution,  
where *redundancy* denotes the 'redund'  
option of running either program *cdd* in



cddlib package [13] or *lrs* in *lrslib*  
package [15]

and those that are non-redundant,

$\text{vertex}(\underline{D}) := \underline{D} - \text{redund}(\underline{D})$  non-redundant or essential vectors

2. Conversions between dual representations of polytope,  $T_v$  in vertices and  $T_h$  in half-planes, of  $\underline{D}$ ,

$T_h(\underline{D}) := \text{half-plane}(\underline{D}) := h\_enum(\text{vertex}(\underline{D}))$  dual half-planes, where *h\_enum* denotes the  
main programs *lrs* or *cdd* from their  
respective packages

$T_v(\underline{D}) := \text{vertex}(\underline{D}) := v\_enum(\text{half-plane}(\underline{D}))$  dual vertices, where *v\_enum* is *lrs* or *cdd*

3. The polytope  $T$  for distribution  $\underline{D}$  of a protein folding class, generally of rank  $r=19$ , is embedded in the 19D hyperplane of the amino acid composition space, for which the content, or volume, is calculated from the vertex set as follows:

$V_T(\underline{D}) := \text{volume}_T(\underline{D})$  volume of polytope  $T$  of  $\underline{D}$ , is the base,  $V_{\text{base}}$ , of the  $(r+1)D$   
pyramid (apexed at the origin of the coordinate system) according  
to the formula

$$V_{\text{pyramid}} = \text{height} * V_{\text{base}} / (r+1)$$

where  $V_{\text{pyramid}}$  is  $\text{volume}(\overline{\text{origin} + \text{vertex}(\underline{D})})$  computed from  
running the program *lrs* in *lrslib* package with the 'volume' option,  
height is  $1/\sqrt{r+1}$ , and  $r$  is the rank of  $\underline{D}$

$V_{T\text{-est}}(\underline{D}) := \text{correl}_r(V_M(\underline{D}))$  where  $\text{correl}_r$  is the correlation relationship in Figure 4 for

rank r

(b) For geometric relationship between distributions  $\underline{D}_1$  and  $\underline{D}_2$  :

4. Polytope intersection, or overlap, of  $T(\underline{D}_1)$  and  $T(\underline{D}_2)$

$$\underline{Q}_p(\underline{D}_1, \underline{D}_2) := v\_enum(T_h(\underline{D}_1) + T_h(\underline{D}_2))$$

vertex enumeration of the combined set  
of half-planes of polytopes for  $\underline{D}_1$  and  $\underline{D}_2$   
that are full rank (r=19)

5. For centroid overlap  $\underline{Q}_c(\underline{D}_1 | \underline{D}_2)$ ,

$$\overline{\text{centroid}}\langle k \rangle := \text{mean}(\underline{\text{Class}}\langle k \rangle)$$

a 20-component vector in the 19D amino acid  
composition space calculated as the mean of  $\bar{v}$ 's for  
vertices of a class distribution. With redundancies  
having been excluded, the centroid is a true  
geometric center, unbiased by any internal  
structure of the distribution or abundance of  
highly repeated or closely related sequences

$$\underline{Q}_c(\underline{D}_1 | \underline{D}_2) := \{ \overline{\text{centroid}}(\underline{D}_2) \text{ if } \text{redund}(\underline{D}_1 + \overline{\text{centroid}}(\underline{D}_2)) == \overline{\text{centroid}}(\underline{D}_2) \}$$

a single  
redundancy test of the vector  $\overline{\text{centroid}}$  of  $\underline{D}_2$   
against distribution  $\underline{D}_1$

6. Distribution overlap,

$$Q_d(\underline{D}_1 | \underline{D}_2) := \{ \bar{v} | \bar{v} \in \underline{D}_2 \text{ \& redund}(T_v(\underline{D}_1) + \bar{v}) == \bar{v} \} \quad N(\underline{D}_2) \text{ single redundancy tests}$$

7. Distribution overlap via stepwise reduction,

$$\underline{D}_{2,i+1} := \underline{D}_{2,i} - \{ \bar{v} | \bar{v} \in \underline{D}_{2,i} \text{ \& vertex}(T_v(\underline{D}_1) + \underline{D}_{2,i}) \}, \text{ where } \underline{D}_{2,0} = \underline{D}_2 \quad \text{identification and}$$

removal of members of distribution  $\underline{D}_2$  that are non-

redundant in the combined set of  $T_v(\underline{D}_1)$  and  $\underline{D}_2$  at a given

step  $i$  ( $\underline{D}_{2,i}$ ), with the process terminating when  $\underline{D}_{2,i}$  are all

redundant or is empty. Even for larger sets  $\text{class}(\mathbf{K})$ , all

calculations are completed in no more than 6 steps

## Supplementary Material

Supplementary material includes a zip archive, *classes.zip*, of five files in plain text: *class-i*,  $i=a,b,c,d,g$ . Each *class-i* file is a list of SCOPe families (labelled in *sccs*'s) constituting the distribution class(*i*). Capitalized *sccs*'s belong in the corresponding Class(*i*). Each record in *class-i* is identified by an *sccs* string, followed by 2 words: (1) amino acid composition in the form of 20 comma-separated fractions, for amino acids in the order of one-letter codes g,a,i,v,l,p,n,k,q,d,e,m,r,c,s,t,h,f,w,y (2) comma-separated SCOPe *sid*'s for the *sccs*.

## Acknowledgment

The author thanks Komei Fukuda, ETH Zurich, author of cdd package, for information on computational geometry and polyhedron calculations early on, and David Avis, McGill U and Kyoto U, author of lrs package, for assistance in lrs software, calculations requiring significant CPU resources, and interest in the project. The author also thanks Barry Honig, Biochemistry, Molecular Biophysics and Systems Biology, Columbia U, for critical reading of the manuscript. Open access to other important and essential resources (minimum volume enclosing ellipsoid procedure and SCOPe database, etc.) are hereby acknowledged.

## References

[1] Levitt M, Chothia C (1976) Structural patterns in globular proteins. *Nature* 261:552–558.

[2] Richardson JS (1981) The Anatomy and Taxonomy of Protein Structure. *Adv Protein Chem* 34:167–339.

Updated Web version at <https://www.semanticscholar.org/paper/The-anatomy-and-taxonomy-of-protein-structure.-Richardson/d848e0df740036b3c8b10371b4624a1599d39191> and <https://dasher.wustl.edu/bio5357/readings/advprotchem-34-167-81.pdf>

[3] Davies DR (1964) A Correlation between Amino Acid Composition and Protein Structure. *J Mol Biol* 9:605-609.

[4] Havsteen BH (1966) A Study of the Correlation between the Amino Acid Composition and the helical Content of Proteins. *J Mol Biol* 10:1-10.

[5] Nakashima H, Nishikawa K, Ooi T (1986) The Folding Type of a Protein Is Relevant to the Amino Acid Composition. *J Biochem* 99:153-162.

[6] Mao B, Chou KC, Zhang CT (1994) Protein folding classes: a geometric interpretation of the amino acid composition of globular proteins. *Protein Eng* 7:319-330.

[7] Orengo CA, Michie AD, Jones S, Jones DT, Swindells MB, Thornton JM (1997) CATH--a hierarchic classification of protein domain structures. *Structure* 5:1093–1108.

- [8] Fox NK, Brenner SE, Chandonia JM (2014) SCOPe: Structural Classification of Proteins—extended, integrating SCOP and ASTRAL data and classification of new structures. *Nucleic Acids Res* 42:D304-309.
- [9] Chandonia JM, Guan L, Lin S, Yu C, Fox NK, Brenner SE (2022) SCOPe: Improvements to the Structural Classification of Proteins—extended Database to facilitate Variant Interpretation and Machine Learning. *Nucleic Acids Research* 50:D553–559.
- [10] Bowman N, Heath MT (2023) Computing minimum-volume enclosing ellipsoids. *Mathematical Programming Computation* 15:621-650.
- [11] <https://gist.github.com/Gabriel-p/4ddd31422a88e7cdf953>, based on work by Nima Moshtagh, <http://www.mathworks.com/matlabcentral/fileexchange/9542>. (download date: 2021-06-21)
- [12] Fukuda K, Prodon A, Double description method revisited. In Deza M, Euler R, Manoussakis I, Ed. (1996) *Combinatorics and Computer Science*, volume 1120 of *Lecture Notes in Computer Science*, Springer-Verlag, pp 91-111.
- [13] Version 0.94m. [https://people.inf.ethz.ch/fukudak/cdd\\_home/](https://people.inf.ethz.ch/fukudak/cdd_home/) <https://github.com/cddlib/cddlib/>
- [14] Avis D (2000) lrs: A Revised Implementation of the Reverse Search Vertex Enumeration Algorithm. In: *Polytopes - Combinatorics and Computation*, Ed. G. Kalai and G. Ziegler, Birkhauser-Verlag, 177-198.
- [15] Version 0.73. <https://cgm.cs.mcgill.ca/~avis/C/lrslib/>
- [16] Nakashima H, Nishikawa K (1994) Discrimination of Intracellular and Extracellular Proteins Using Amino Acid Composition and Residue-pair Frequencies. *J Mol Biol* 238:54-61.

- [17] Chou KC (2001) Prediction of protein cellular attributes using pseudo-amino acid composition. *Proteins* 43:246-55.
- [18] Cedano J, Aloy P, Pérez-Pons JA, Querol E (1997) Relation between amino acid composition and cellular location of proteins. *J Mol Biol* 266:594-600.
- [19] Chou KC (2011) Some remarks on protein attribute prediction and pseudo amino acid composition. *J Theor Biol* 273:236–247.
- [20] Jumper J, Evans R, Pritzel A, Green T, Figurnov M, Ronneberger O, Tunyasuvunakool K, Bates R, Židek A, Potapenko A, Bridgland A, Meyer C, Kohl SAA, Jain R, Adler J, Back T, Petersen S, Reiman D, Clancy E, Zielinski M, Steinegger M, Pacholska M, Berghammer T, Kohli P, Hassabis D (2021) Highly accurate protein structure prediction with AlphaFold. *Nature* 596:583-589.
- [21] Kendall MG (1961) *A course in the geometry of n dimensions*, Hafner Pub. Co., New York.
- [22] Michie AD, Orengo CA, Thornton JM (1966) Analysis of domain structural class using an automated class assignment protocol. *J Mol Biol* 262:168-185.
- [23] Brenner SE, Chothia C, Hubbard TJP, Murzin AG (1996) Understanding protein structure: Using SCOP for fold interpretation. Chap. 37 in: Doolittle RF, ed. *Computer Methods for Macromolecular Sequence Analysis*. *Methods in Enzymology*. Vol. 266. Orlando, FL: Academic Press. 635-643.
- [24] Murzin AG, Brenner SE, Hubbard TJP, Chothia C (1995) SCOP: a structural classification of proteins database for the investigation of sequences and structures. *J Mol Biol* 247:536-540.



- [25] <https://scop.berkeley.edu/downloads/update/{dir.cla.scope.txt,dir.com.scope.txt}> (download date: 2024-04-24)
- [26] <https://scop.berkeley.edu/downloads/scopeseq-2.08/astral-scopedom-seqres-gd-all-2.08-stable.fa> (download date: 2024-04-24)
- [27] <https://scop.berkeley.edu/astral/seq/ver=2.08&seqOption=0&output=text&id=sid>, where sid is the 7-character domain identifier for those that are absent in the the astral file (fetch date: 2024-04-30)
- [28] Zhang CT, Zhang R (1998) A new quantitative criterion to distinguish between  $\alpha/\beta$  and  $\alpha+\beta$  proteins (domains). FEBS Letters 440:153-157.
- [29] Potenza E, Di Domenico T, Walsh I, Tosatto SCE (2015) MobiDB 2.0: an improved database of intrinsically disordered and mobile proteins. Nucleic Acids Res 43:D315-320.

## Figure Legends

### Figure 1

Geometric representations of a data distribution in 2D. The distribution is a point set consisting of 10 vertices (light gray) and 7 interior points (dark gray), and a descriptive model of the distribution is a geometric object that best covers the point set. For protein folding classes, each point in the distribution is the endpoint of an amino acid composition vector. In computational geometry calculations [12-15], the convex polytope is defined either as the set of 10 vertices, or as its dual, the set of 10 inequality equations (one of which is shown as a half-plane in dashed lines). For the three models, pmmd and mve ellipses (ellipsoid and hyper-ellipsoid in higher dimensions) and polytope, the areas (volume and hyper-volume in higher dimensions) are 0.2695, 0.0523, and 0.0353, respectively. Of the three models, removal of the 7 interior points from the distribution changes only the pmmd ellipse, reducing the area to 0.2191, but has no effect on the mve ellipse or the polytope (hence rendering such interior points 'redundant' therefor).

### Figure 2

Schematic drawing of pair-wise relationships between polygons (polytopes in 2D). In general when two full-rank polytopes (blue and green) intersect, the overlap is itself a polytope, i.e. the region marked in orange and defined by five vertices (circles) to be enumerated from the combined set of half-planes (dashed lines in blue and green). For polytopes of large number of vertices and half-planes, vertex enumeration is computationally demanding and provisional overlap information can be derived from discrete levels of overlap: (1) full centroid overlap (blue and red polygons), when the polygons are sufficiently close such that each envelope encloses the other centroid; (2) partial centroid overlap

(green and red), when only one polytope encloses the other centroid; (3) distribution overlap (blue and green), with or without any centroid overlap, when one polytope encloses some vertices and/or interior points of the other. Formal definitions are found in Methods II(b). Further, polytopes in higher dimensions may yet overlap only at facets: facet overlap (orange), for example two 3D prisms in contact at the long edges. Schematically for class  $k$  of SCOPe database,  $T(\text{class}\langle k \rangle)$  is shown in solid blue lines, two of its Family $\langle s \rangle$  in dotted lines (the families with  $N$  of 4 and rank 2, and  $N$  of 2 and rank 1 respectively, and their members marked by  $\times$ ), and  $T(\text{class}\langle k_0 \rangle)$  in short dashed lines.

Figure 3

SCOPe hierarchy, reproduced with permission, from <https://scop.berkeley.edu/help/ver=2.08>.

Figure 4

Top: Linear correlation between  $V_M(\underline{D})$  and  $V_T(\underline{D})$  for  $\underline{D}=\text{family}\langle s \rangle$  in SCOPe database,  $N(\underline{D}) \leq 51$  and rank=19 (222 data points), and  $\underline{D}=\text{class}\langle J \rangle$  (4 data points). The 95% confidence interval of prediction for the regression is shaded in gray. Bottom: regression coefficients. Enclosed in parentheses are the number of data points for a given rank (columns 1 and 4), and the coefficients and the standard errors in parentheses (columns 2,3, and 5,6).

Figure 5

Comparison of amino acid compositions for folding types  $\alpha$  and  $\beta$ . Top panel: Deviations for class $\langle 1 \rangle$  and class $\langle 2 \rangle$ , computed from the overall centroid of all proteins in NNO basis set. This is comparable to Figure 1 in [5], except for the slightly different Y-scale due to plain, un-normalized composition vectors in this study, and minor differences due to computing in rational number arithmetic.

Comparison of distributions between folding classes or between different datasets is simpler and more straightforward in the amino acid composition space of plain amino acid fractions without normalization. Bottom panel: Deviations for  $\text{class}\langle a \rangle$  and  $\text{class}\langle b \rangle$ , computed from  $\overline{\text{centroid}(\text{centroid}\langle \mathbf{L} \rangle)}$ , with a slightly smaller Y-range, and a different horizontal order of amino acids. For completeness the total bar length in unit of standard deviation for each amino acid is noted below the single-letter code.

Figure 1. Geometric models (2D data distribution)

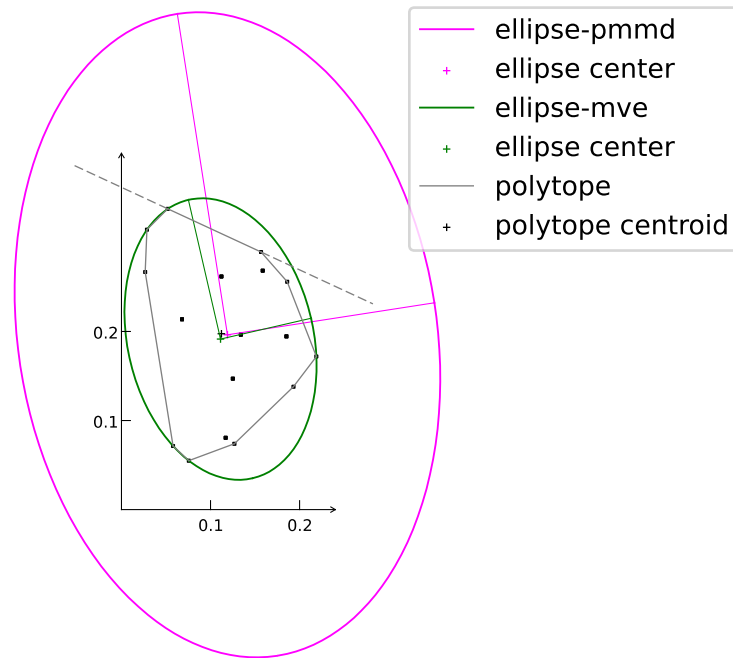


Figure 2. Polytope overlaps

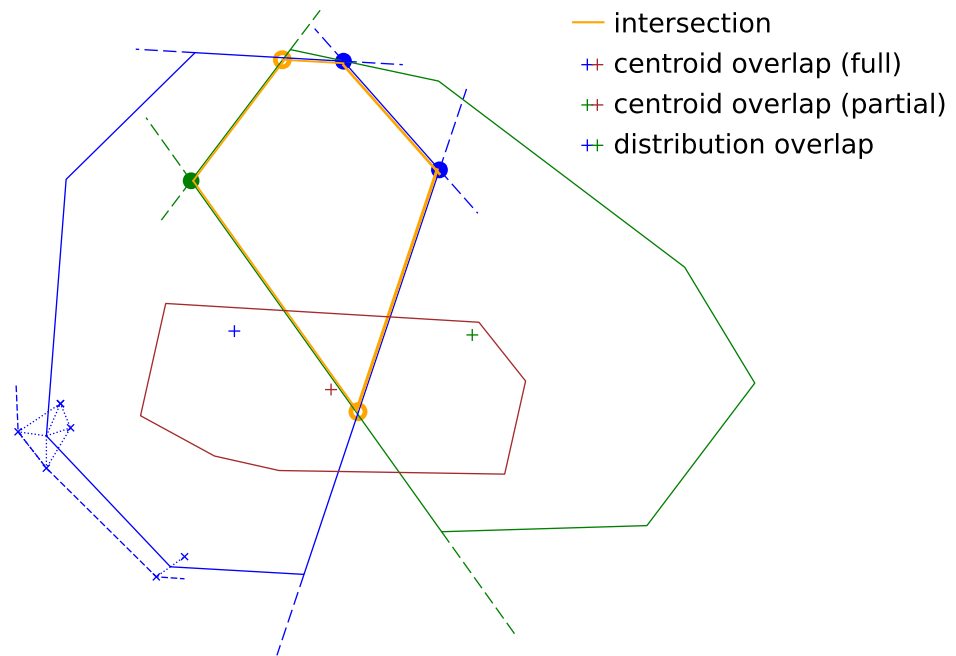


Figure 3. SCOPe hierarchy

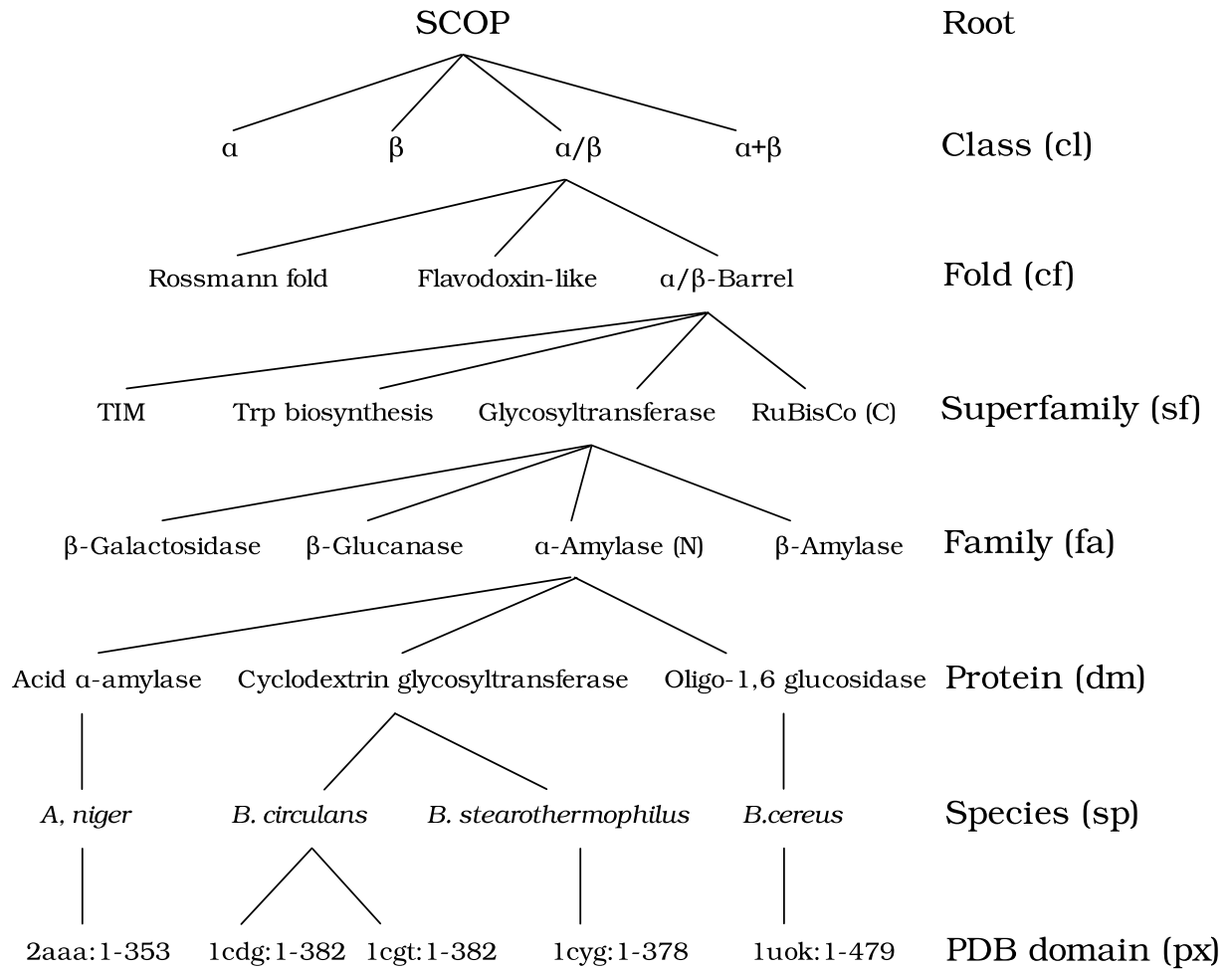
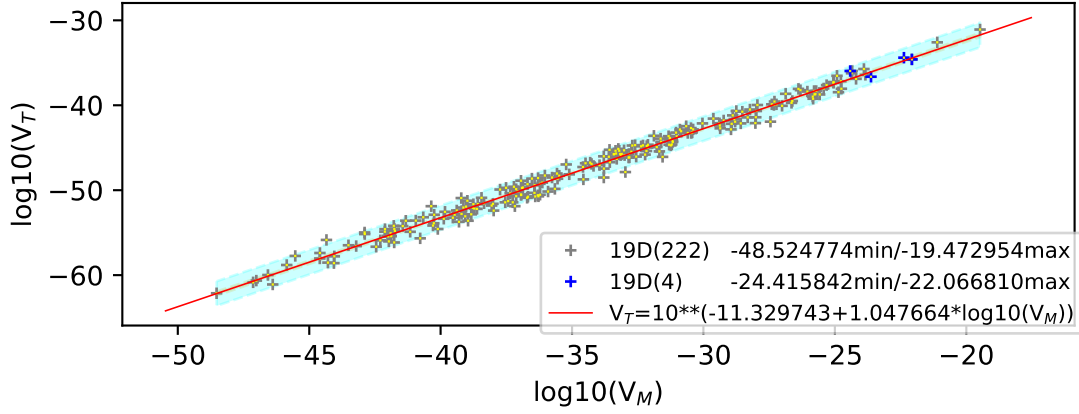


Figure 4. Correlation of  $V_M$  and  $V_T$



10D( 85)	-10.305(0.859)	0.868(0.024)	19D(226)	-11.330(0.778)	1.048(0.008)
9D( 87)	-10.209(0.910)	0.822(0.029)	18D( 36)	-15.280(1.846)	0.953(0.040)
8D( 97)	-8.893(0.913)	0.834(0.030)	17D( 40)	-13.743(1.401)	0.978(0.031)
7D(122)	-7.444(0.789)	0.858(0.028)	16D( 43)	-15.896(1.479)	0.898(0.034)
6D(134)	-6.586(0.746)	0.832(0.030)	15D( 35)	-13.386(1.622)	0.953(0.041)
5D(183)	-5.712(0.651)	0.807(0.026)	14D( 62)	-13.682(1.194)	0.914(0.029)
4D(251)	-4.651(0.647)	0.802(0.026)	13D( 56)	-12.883(1.122)	0.899(0.028)
3D(261)	-4.000(0.509)	0.723(0.025)	12D( 65)	-12.164(1.034)	0.884(0.028)
2D(362)	-3.175(0.424)	0.621(0.024)	11D( 66)	-12.122(0.919)	0.847(0.026)



Figure 5. Amino acid compositions,  $\alpha$  vs  $\beta$

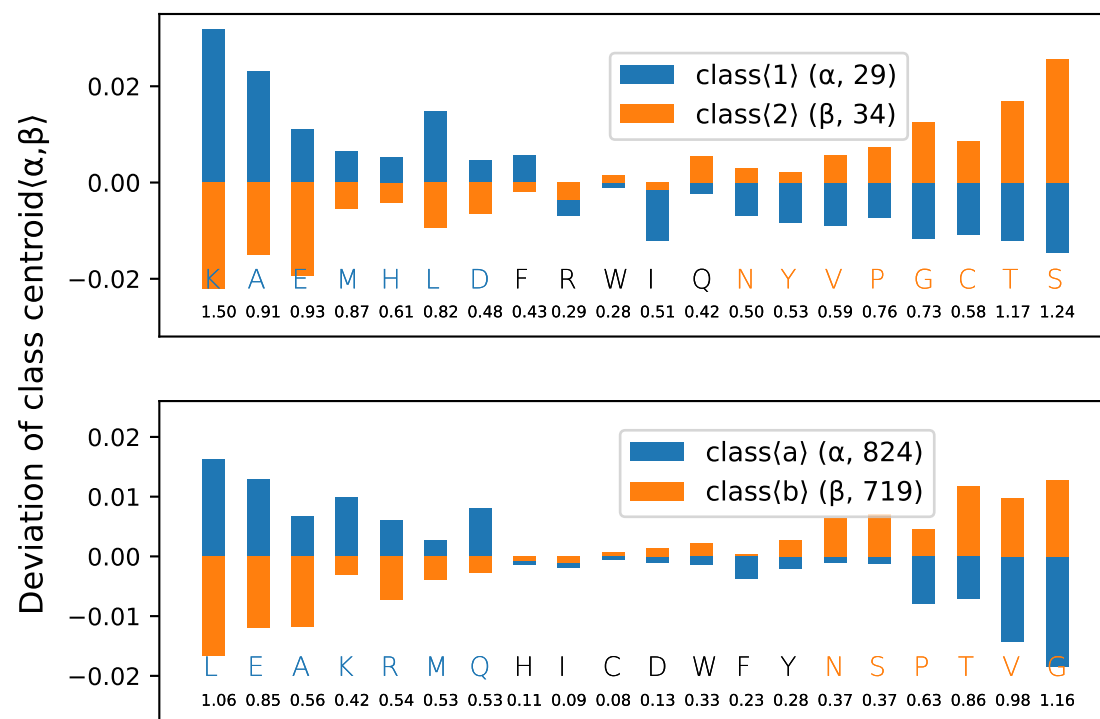


Table I. Geometric parameters of data distributions  
NNO basis set of Nakashima et al.

protein folding type		$\alpha$	$\beta$	$\alpha/\beta$	$\alpha+\beta$	(irregular proteins)
		class(1)	class(2)	class(3)	class(4)	class(5)
	N(class(i))	29	34	39	26	4
pmmd ellipsoid*	volume	3.168e-21	4.959e-21	1.366e-22	3.702e-23	na
mve ellipsoid	volume	8.574e-23	4.257e-23	3.838e-25	2.369e-24	na
	radii,range	0.013~0.276	0.019~0.246	0.019~0.186	0.011~0.272	na
	aspect ratio	20.52	18.87	9.64	24.77	na
polytope	N(vertex(i))	29	34	39	26	na
	N(half-plane(i))	102472	1124858	6192246	18182	na
	volume	2.455e-35	4.003e-35	1.059e-36	2.256e-37	na

The aspect ratio is the simple ratio of longest semi-axis radius to the shortest, as a measure of ellipsoid shape. For class(5), there are only 4 proteins, not full-rank and thus without volume and polytope data in the amino acid composition space.

\*Although pmmd ellipsoid is deprecated in this study, the volume data are reproduced for backward reference and for comparison here. They are corrected from previously published values which had been calculated from only the product of ellipsoid radii, the third term in expression 14 [6]. The multiplicative factor of 0.0466 (due to first two terms) has been applied for correction. Values above also differ by a slight increase of precision due to rational arithmetic, and a factor of e-38 due to unit change from percent to simple fraction.

Table II. Pre-processing (a) and statistics (b) of protein structure data from SCOPe database, version 2.08 with 2023-1-6 update

a. pre-processing						
		class(cl) = a~l	cl = a~d,g	cl = a~d,g fa ≠ 0		
<b>dir.cla</b>	structure domain (px)	348214	290961	210541 (196826‡)		
	protein (dm)	13526	12258	11363 (11121‡)		
	family (fa)	5433	4754	3859 (3796‡)		
px amino acid sequences				<b>astral</b> : 208681 <b>wget</b> : 1860		
incomplete or short sequences				Incomplete: 5728 23 residues or fewer: 59		
				px count final: 204754 dm count final: 11100 fa count final: 3789		

b. statistics						
protein folding type		$\alpha$	$\beta$	$\alpha/\beta$	$\alpha+\beta$	small proteins
class		a	b	c	d	g
full database	px (total 290961)	44921	77485	84681	76691	7183
	dm (total 12258)	2490	2610	3085	3276	797
	fa (total 4754)	1089	993	1003	1388*	281*
pre-processing	px (total 204754)	32957	55705	53404	56681	6007
	dm (total 11100)	2285	2333	2773	2966	743
	fa (total 3789)	893 (895‡)	766 (777‡)	807 (826‡)	1093 (1086‡)	230 (236‡)
	px count, per fa distribution	N(family(s))	1~2750	1~7754	1~1922	1~7211
		N(Family(s))	1~528	1~2800	1~702	1~1627

**Pre-processing**, proceeding first from left to right, rows 1-3, then top to bottom, column 3. Three streams of data (highlighted in bold) are sourced from SCOPe: **dir.cla** [23], **astral** [24], and **wget** [25]. Class, protein structure domain, protein and family are levels of the SCOPe classification hierarchy, their two-letter code in parentheses in part a. SCOPe family of level '0' (namely SCOP concise classification string of cl.cf.sf.0) are automatic matches and not true families (as noted in the comment file dir.com.scope.txt), and thus excluded. Incomplete sequences are those that contain one-letter amino acid residue code x, for unknown, undetermined, or non-naturally occurring amino acid residues, for which the amino acid composition vectors are anomalous (the 20 components for the essential amino acid residues do no sum to 1). Lastly, there are a small number of instances of asp/asn (32) and glu/gln (48) ambiguous pairs, in 9 px sequences, labelled with one-letter code of b and z respectively. In each group, half of the instances are assigned to one of the two residues in the pair, and the other half to the second residue.

**Statistics**. Full database, rows 1-3, correspond to rows 1-3, column 2 in a. **pre-processing**, rows 4-6, correspond to rows 9-11, column 3 in a.

‡From file dir.cla.scope.2.07-2020-07-16.txt downloaded on 2020-07-21. Pre-processing did not include short sequences and ambiguous asp/glu pairs.

\*Family counts for classes d and g parsed from **dir.cla** are each 1 higher than listed in SCOPe online Statistics.

Table III. Geometric parameters of full and interior data distributions  
SCOPe-2.08-2023-01-06

a. full distribution

protein folding type		$\alpha$	$\beta$	$\alpha/\beta$	$\alpha+\beta$	(small proteins)
		class(a)	class(b)	class(c)	class(d)	class(g)
	N(class(k))	893 (895‡)	766 (777‡)	807 (826‡)	1093 (1086‡)	230 (236‡)
mve ellipsoid	volume	5.523e-18	2.118e-18	1.975e-21	1.418e-18	4.721e-17
	radii, range	0.071~0.324	0.060~0.334	0.040~0.259	0.053~0.284	0.073~0.405
	dim <sub>M</sub> (class(k))	0.145	0.137	0.096	0.135	0.162
	aspect ratio	4.56	5.59	6.53	5.35	5.54
polytope	N(Class(k))	824 (819‡)	719 (723‡)	744 (753‡)	993 (981‡)	229 (228‡)
	volume, est.	3.884e-30	1.423e-30	9.513e-34	9.343e-31	3.678e-29

b. interior distribution

N(D)		69	47	63	100	1
mve ellipsoid	volume	9.222e-28	7.170e-29	2.983e-31	6.708e-28	na
	radii, range	0.017~0.117	0.013~0.105	0.010~0.087	0.021~0.106	na
	aspect ratio	6.86	8.01	8.89	4.99	na
polytope	N(vertex(D))	69	47	63	100	na
	volume, est.	2.216e-40	1.525e-41	4.885e-44	1.588e-40	na
	centroid shift	0.012	0.009	0.009	0.007	na

Estimated polytope volumes (row 7 in a. **full distribution** and row 6 in b. **interior distribution**) were calculated from the regression formula for 19D in Figure 4. The interior distributions for class(L) are all vertices without redundancy, and for class(g), N of 1 and no polytope (rows 1 and 5 in b.). For interior polytopes of classes L, the centroid shifts (row 7, **interior distribution**) are calculated relative to centroids of the respective main polytope (those from row 6, **full distribution**). These shifts are small in comparison to the dimensions of the full distributions (rows 3,4, **full distribution**), indicating that (a) the interior polytopes are nearly concentric with the respective full polytopes, and (b) class(L) distributions are essentially 2-layered geometric structures.

‡Data for SCOPe-2.07-2020-07-16; see Table II for data pre-processing.

Table IV. Distribution overlap, centroid overlap and distances

## a. Distribution overlap

$k'$ \ $k$	class(a), 893	class(b), 766	class(c), 807	class(d), 1093	class(g), 230
Class(a), 824		16(10)	114(70)	59(12)	0
Class(b), 719	4(1)		96(52)	41(4)	0
Class(c), 744	2(0)	3(0)		18(1)	0
Class(d), 993	25(5)	52(25)	195(132)		0
Class(g), 229	0	0	0	0	
Class(K)	25(5)	55(28)	223(160)	85(17)	0

## b. Centroid overlap and distances

$k'$ \ $k$	Class(a)		Class(b)		Class(c)		Class(d)		Class(g)	
Class(a)			no	*	yes	*	yes	*	no	*
Class(b)	no	0.0696			yes	*	yes	*	no	*
Class(c)	no	0.0443	yes	0.0391			yes	*	no	*
Class(d)	yes	0.0399	yes	0.0343	yes	0.0171			no	*
Class(g)	no	0.1244	no	0.1080	no	0.1164	no	0.1120		
centroid(centroid(L))		0.0372		0.0343		0.0153		0.0073		0.1122
Class(J)		0.0687		0.0579		0.0263		0.0552		
(2.07-2020-07-16)		0.0008		0.0011		0.0009		0.0007		0.0013

**Distribution overlap.** Rows 1 to 5:  $O_d(\text{Class}(k')|\text{class}(k))$ , of class( $k$ ), labelled at the top, against Class( $k'$ ), labelled on the left. Labels are followed by the number of families in the class. For each entry of the table the number in parentheses are vertex counts. Row 6: distribution overlap between class( $k$ ) and Class(K).

**Centroid overlap and distances.** Rows 1 to 5: centroid overlap, yes/no (asymmetric,  $O_c(\text{Class}(k')|\text{Class}(k))$ ), and centroid-to-centroid distances (symmetric). Row 6: distance of Class( $k$ ) centroid to the group centroid of four major folding types. NB, distances from group centroid to Class(a) and Class(b) sum up to be about the distance between Class(a) and Class(b). Row 7: distances between Class( $k$ ) and corresponding folding type of NNO basis set. Row 8: distance of Class( $k$ ) centroid from the corresponding folding type in SCOPE-2.07-2020-07-16 dataset.

\*Symmetric distance equal to that from Class( $k'$ ) to Class( $k$ ).